The role of LSWS (satellite traces) and low latitude E_{sb} layers in causing the variability of ESF irregularities over Indian sector

Sreeba Sreekumar *, S. Sripathi

Indian Institute of Geomagnetism, Plot-5, Sector-18, New Panvel, Navi Mumbai, India

Abstract

We investigate the ionogram signatures of LSWS (satellite traces) and low latitude E_{sb} layers as a basis for causing variabilities of ESF irregularities in addition to post sunset vertical drift using ground based ionosondes located at Tirunelveli (8.71°N, 77.75°E, Geomag. Lat 0.21°N) and Hyderabad (17.38°N, 78.48°E, Geomag. Lat 8.74°N) for the year 2015. Results show, statistically, that the presence/ absence of STs are higher/lower than the absence/presence of E_{sb} prior to occurrence/non-occurrence of ESF during all the seasons. This implies the importance of ST/LSWS in the ESF occurrence. Results of weak correlation of low latitude E_{sb} layers with ESF possibly indicate its coupling to higher apex altitude than base of the F-layer. Significant equinoctial asymmetry is also observed in both the ESF and ST occurrences wherein vernal is dominant than autumn equinox. Band-pass filtered h'F oscillations of 1–1.5 h reveal significant wave amplification during the PRE on ESF than non-ESF days and also during vernal than autumn equinox. Further investigations suggest that the height oscillations of early ESF and delayed ESF are amplified according to their onset time of ESF. The study suggests that post-sunset height rise of F-layer together with the presence of LSWS provide suitable conditions for the ESF development. Further, the presence of downward phase propagation on ESF days than other days indicate the presence of upward propagating Gravity Waves in the initiation of these wave structures.

© 2018 COSPAR. Published by Elsevier Ltd. All rights reserved.

1. Introduction

The night time plasma density irregularities over magnetic equator are often denoted as equatorial spread F (ESF) (Kelley et al., 2011). They cause radio wave scintillations that degrade communication and navigation systems and hence understanding the generation mechanism, characteristics and variabilities of these irregularities are important for its prediction. This in turn can facilitate the smooth functioning of radio communication and navigation systems. These irregularities are an outcome of the Rayleigh Taylor (RT) instability mechanism which operates under the condition of a heavy fluid (denser F region) resting on the top of a light fluid (lesser dense region below F region). This occurs as a result of F region height rise due to Pre-Reversal Enhancement (PRE) as well as due to the recombination of E region densities during sunset hours. Under the favorable conditions, any seed perturbation (such as gravity wave (GW)) present will result in RT instability growth. The ESF irregularities show long, medium and short term variabilites. While long term variations are attributed to solar and geomagnetic activity differences, medium and short term variations represent seasonal and day to day variabilities. Most of these short term variations are caused by the atmospheric forcing arising from lower atmosphere. It is believed that while post sunset height rise is important parameter for the causes

---

* Corresponding author.
   E-mail address: sreebask12@iigs.iigm.res.in (S. Sreekumar).

of day-to-day variability of ESF irregularities, recently it has been reported that other parameters such as low latitude E region conductivities, trans-equatorial/meridional winds etc also play important role in day-to-day variability (Fejer et al., 1999; Abdu et al., 1983; Maruyama, 1998).

Apart from these factors the very initiative process provided by seed perturbation in causing faster growth of RT instability is of great importance. Understanding the day to day variabilities of ESF is an active subject since many years especially from the perspective of seeding by LSWS/GW. Most known source of seed perturbation is the presence of gravity waves (GWs) in the evening thermosphere (Kelley et al., 1981; Takahashi et al., 2009). These waves are believed to be originated from lower atmospheric regions and propagated to ionospheric heights. The significant presence of GWs during ESF events were studied by Abdu et al. (2009). From Indian sector, the GW perturbations on ESF days were reported by (Sreeja et al., 2009; Taori et al., 2010; Patra et al., 2013; Manju et al., 2016), etc. More recently, Li et al. (2016) reported the increased plasma bubble generation at an equatorial longitude, Kototabang. They attributed this to a higher GW activity associated with the more active Intertropical Convergence Zone (ITCZ). It is believed that GWs can modulate the post sunset F-layer heights through large undulations in iso electron density-lines (refers to curves of equal electron density), wherein the elevated bottom-side density gradient regions become unstable to generalized RT instability.

Another representation of the precursor wave modulation is through the quasiperiodic large-scale wave structure (LSWS). Tsunoda and White (1981) reported that LSWS can be identified as quasiperiodic modulation in the altitude of isoelectron density contours in the bottomside F-region, superimposed on a mean slope that increases in altitude from west to east; the latter is consistent with the PSSR. The zonal scale length of the order of a few hundred kilometers have been detected by east-west scanning VHF radars (Tsunoda, 2005, 2008), TEC measurements (Thampi et al., 2009; Tulasi Ram et al., 2012) and airglow images (Narayanan et al., 2012). The significance of these structures arise due to the fact that they are considered as manifestations of the seed perturbation favouring the RT instability growth and thereby generation of ESF. Over the years, various reports suggest the evidence of presence of LSWS in the bottom side of the F region prior to the onset of Equatorial Plasma Bubbles (EPBs) (Tsunoda, 2008; Thampi et al., 2009). These zonal structures along with PRE is believed to have a control on the onset and location of ESF (Tsunoda and White, 1981; Saito and Maruyama, 2007; Kherani et al., 2009). However, using the ALTAIR radar observations over Kwajalein Atoll, Tsunoda (2005) found that the ESF tended to be more closely related to the occurrence of LSWS than to the strength of PRE. Recently, Abdu et al. (2009) reported that the height oscillations as a result of LSWS, as seen at the F layer bottomside plasma frequencies revealed the properties of upward propagating GW signatures. These oscilla-

tions started appearing around afternoon hours and their growth enhanced during PRE in the post sunset period leading to plasma bubble irregularities.

The validation of a phenomena becomes more easier, if it can be observed by various instruments as different manifestations. Other than previously discussed ground and space based instruments, ionosondes can be also used to understand various signatures of LSWS. It is suggested that small tilts in F layer can be used as signatures of LSWS in ionograms known as Satellite Traces (STs) (Abdu et al., 1981; Tsunoda, 2008), highly tilted traces called MRE (Multi reflected echoes) as reported (Tsunoda, 2009; Thampi et al., 2012) or fork traces (Lyon et al., 1961). Abdu et al. (1981) showed that always satellite traces preceded range type spread-F (RSF) in the ionograms over an equatorial station, Fortaleza. More recently, the relationship between ST and ESF generation was studied by various researchers (Li et al., 2012; Narayanan et al., 2014).

Another causative factor for the day to day variability discussed in the study is the association of blanketing sporadic E (E_{sb}) layers over low latitude station, HYD to the ESF occurrence. The presence of thin layers of enhanced ionization at E region heights of 100–120 km are known as sporadic E (E_s). Near the magnetic equator, the E_s observed is patchy and transparent to waves reflected from the higher layers. Sometimes these layers are highly dense known as blanketing type sporadic E (E_{sb}) and they can effectively block the upper ionospheric layers to the radio waves. Using modeling related studies, strong connection between the low-latitude E region field-line integrated Pedersen conductivity and the onset of RT instability leading to spread F bubbles has been shown by Stephan et al. (2002) and Bhattacharyya (2004). Batista et al. (2008) suggested the absence of any correlation between ESF occurrence at the magnetic equator and the presence of E_s layers at the conjugate E regions. Recently, the importance of low latitude E_s in varying the total field-line integrated Pedersen conductivity that affects the growth rate of RT instability was discussed by Joshi et al. (2013) especially for the cases where F layer is at an altitude of 300–360 km.

The various parameters mentioned above have been studied individually in previous reports and linked to the variabilities associated with ESF. However their comparative/complementary roles in affecting the ESF generation have been not discussed much in the past particularly in understanding the equinoctial asymmetry in the ESF occurrence. A few authors have explained the asymmetry in terms of change in the neutral composition, difference in the solar flux dependence, differences in electron densities, neutral winds etc (Sripathi et al., 2011). However, other than these factors, seeding (LSWS/GW) as well as the presence/absence of E_{sb} might also contribute to the differences in ESF over two equinoxes through its effect in the RT instability term.

In this paper, we present the characteristics of ionogram signatures of LSWS and ESF occurrences over Tirunelveli

on a seasonal basis. Further, we analyzed the competitive role of E_{sb} layers over Hyderabad and STs over Tirunelveli during different seasons statistically in providing necessary conditions for the generation of ESF irregularities in addition to post sunset height rise due to PRE. The study also examines the equinoctial asymmetry of ESF occurrences in the perspective of STs and E_{sb} layers along with PRE in affecting the ESF development/suppression. We believe this kind of consolidated study is a first of its kind specially from the perspective of Indian region. Additionally as a supporting evidence, we also present the characteristics/ significance of LSWS case by case, eg: during presence of ESF, absence of ESF, early ESF and late ESF onset cases using band pass filtered height oscillations. We believe this kind of analysis helps in validating the results of ST statistics. and has not been presented before. The gravity wave propagation characteristics in relation with wave structures is also included in the study. Thus we attempt to relate the competing/complementary factors such as PRE, LSWS and E_{sb} layers in affecting the variabilities associated with ESF irregularities.

2. Data and methods of analysis

The study presented in the paper are obtained from Canadian Digital Ionosondes (CADI) data from Tirunelveli (TIR) (8.71°N, 77.75°E, geomag.Lat 0.21°N), an equatorial station, and a low latitude station, Hyderabad (HYD) (17.38°N, 78.48°E, geomag.Lat 8.74°N) during the year 2015 which is a moderate solar activity period. The data analyzed covers the period of March – April (March – April (MA)), June – July – August (JJA), September – October (September – October (SO) and November-December (November – December (ND)) seasons. The ionograms collected at every 10 min interval from these two ionosondes form the basis of the analysis. Based on the ionosonde data from TIR, presence/absence of ESF is visually identified. Later on, ESF onset times and occurrence durations for each season are noted. Further, h'F (km) values are scaled. We are discussing only the ESF occurrences/non occurrences at TIR. The various ionogram signatures of LSWS such as ST/MRE/fork traces (at TIR) for different seasons are identified through visual inspection of ionograms and corresponding statistics is made. STs are known as copies of the normal F-layer traces that generally appear above or below the main F-layer trace and produced by one or more reflections from the bottomside of the F layer (Abdu et al., 1981). The presence of highly tilted traces in ionograms are known as MRE and they are probable signatures of larger scale tilts than those that could have resulted in the formation of ST (Tsunoda, 2012). Fork traces are observed as the branching of the F trace near the critical frequency. All the ST occurrences within 2 h are considered as one ST event (Narayanan et al., 2014). The ST signatures separated in excess of 2 h are considered as separate ST events. Further,

we have considered that ST and ESF are related only if the ESF is observed within 2 h of the last observation of ST.

Fig. 1 shows the example of different types of ionogram signatures of LSWS namely, (a) ST (b) MRE and (c) fork traces. Since the presence of MRE/fork trace is comparatively lesser than ST's, we mainly consider ST's in the overall analysis. Fig. 2 shows the magnetic field geometry of the equatorial and low latitude ionosphere. The red lines denotes the south to north magnetic field lines. Apex altitude refers to the height above the equatorial station. This figure represents the linkage of low latitude (HYD) E_{sb} and equatorial (TIR) ESF through field line geometry, i.e., how well the field lines over HYD are connectd to TIR. It may be mentioned that the field-line integrated Pedersen conductivity of the E region (100–150 km) over HYD connect to the bottom of the F region (240–290 km) via magnetic field lines over the magnetic equator (TIR), where seeding of the RT instability takes place. Hence, the E region observations from HYD may prove helpful in understanding the low-latitude E_{sb} activity to some extent and its effect
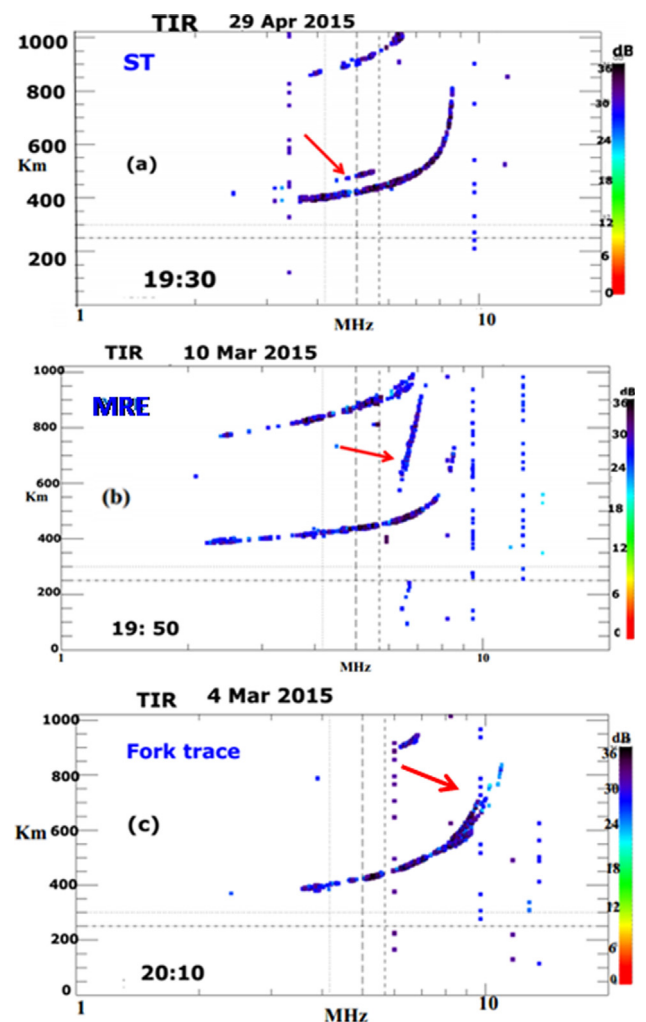

Fig. 1. Ionogram signatures (at equatorial station, Tirunelveli, TIR) of LSWS – (a) Satellite Traces (ST), (b) Multi Reflected Echoes (MRE), (c) Fork Traces.
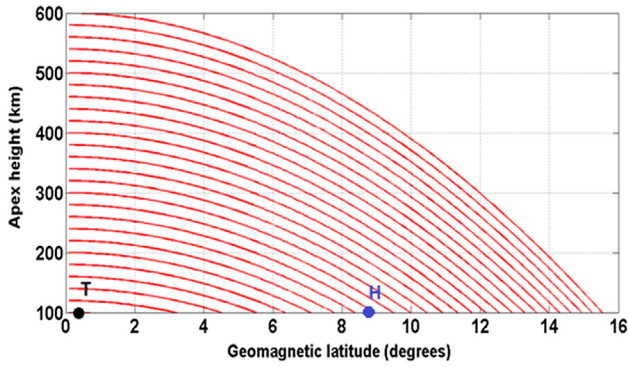
Fig. 2. Magnetic field line configuration in the equatorial and low latitude ionosphere. The black and blue dots denote the geomagnetic latitude of TIR (T) and HYD (H) respectively. (For interpretation of the references to colour in this figure legend, the reader is referred to the web version of this article.)

on the ESF. Present study deals with the type of sporadic E known as blanketing E_s layers (E_{sb}) in the HYD region. The E_{sb} layers during post sunset hours prior to ESF onset is also scaled for which ionosonde data from HYD station is made use of. Accordingly, E region parameters such as ftEs, the top frequency of E_s and fbEs, the blanketing frequency are obtained. Fig. 3 shows the typical examples of E_s and E_{sb} layers over HYD as seen during 2015.

Additionally, to understand the characteristics of LSWS precursor signatures which are believed to be induced by

GWs, height values were band-pass filtered so as to extract their oscillation amplitudes as wave structures within a period band from 1 to 1.5 h. To serve the purpose, the scaling of h'F at fixed frequencies of 5, 6 and 7 MHz is performed. Moreover, to understand the GW propagation characteristics, parameter foF2 is scaled for different sets of fixed height values from 250 km to 350 km and Fast Fourier ransform (FFT) is performed to extract the time period of GWs. Detailed discussion of the results are incorporated in the following sections.

3. Observations and results

3.1. Characteristics and association of ESF and satellite traces (STs)

Fig. 4a–d represents the statistics of ionogram signatures of LSWS and ESF occurrences over TIR during the year 2015. The blue colour lines denote ESF durations, while red, black and green coloured lines indicate the ST, MRE and fork traces as seen on multiple ionograms. The red, black and green stars denote ST, MRE and fork traces as seen on a single ionogram. Yellow and cream lines represent data gap and disturbed days respectively. The white gap in between the lines indicate the absence of ESF. It may be also mentioned that Ap > 15 is considered as disturbed days. A near similar general criterion is used in previous literatures (Narayanan et al., 2014). For this sector,
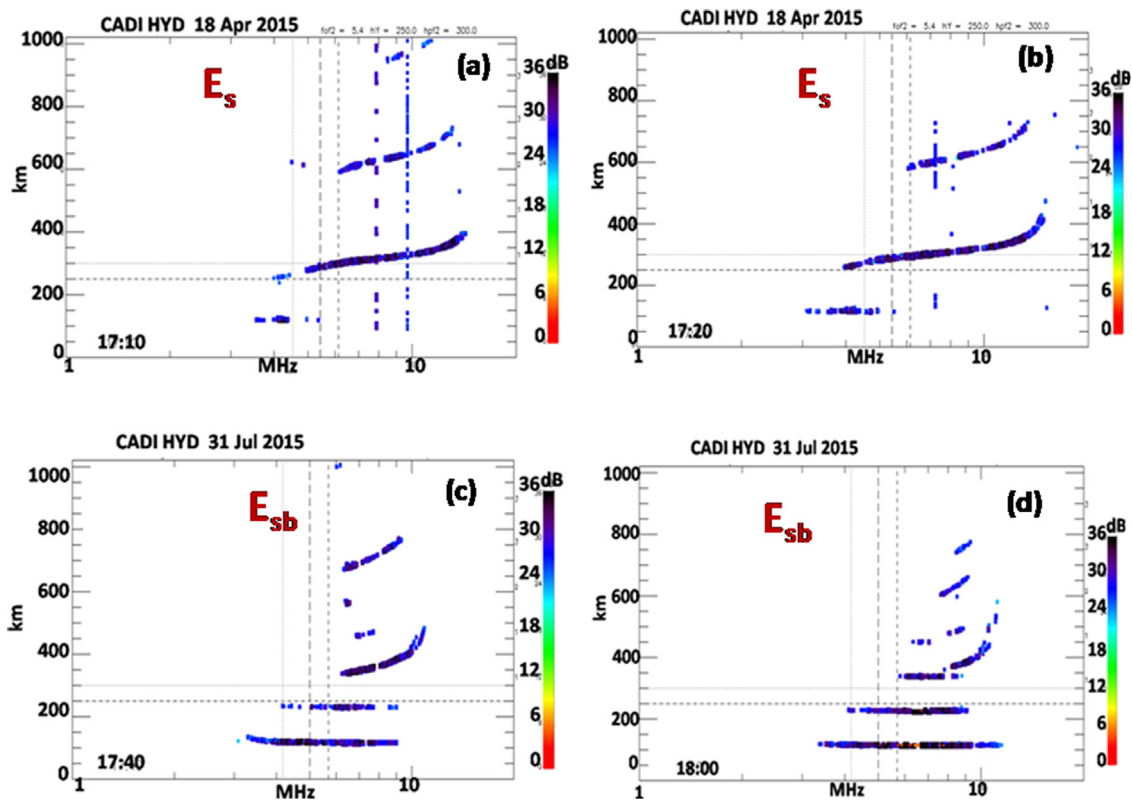

Fig. 3. A few examples of (a) and (b) E_s layers on a typical day (18 April 2015), (c) and (d) E_{sb} layers on a typical day (31 July 2015) over low latitude station, Hyderabad (HYD).
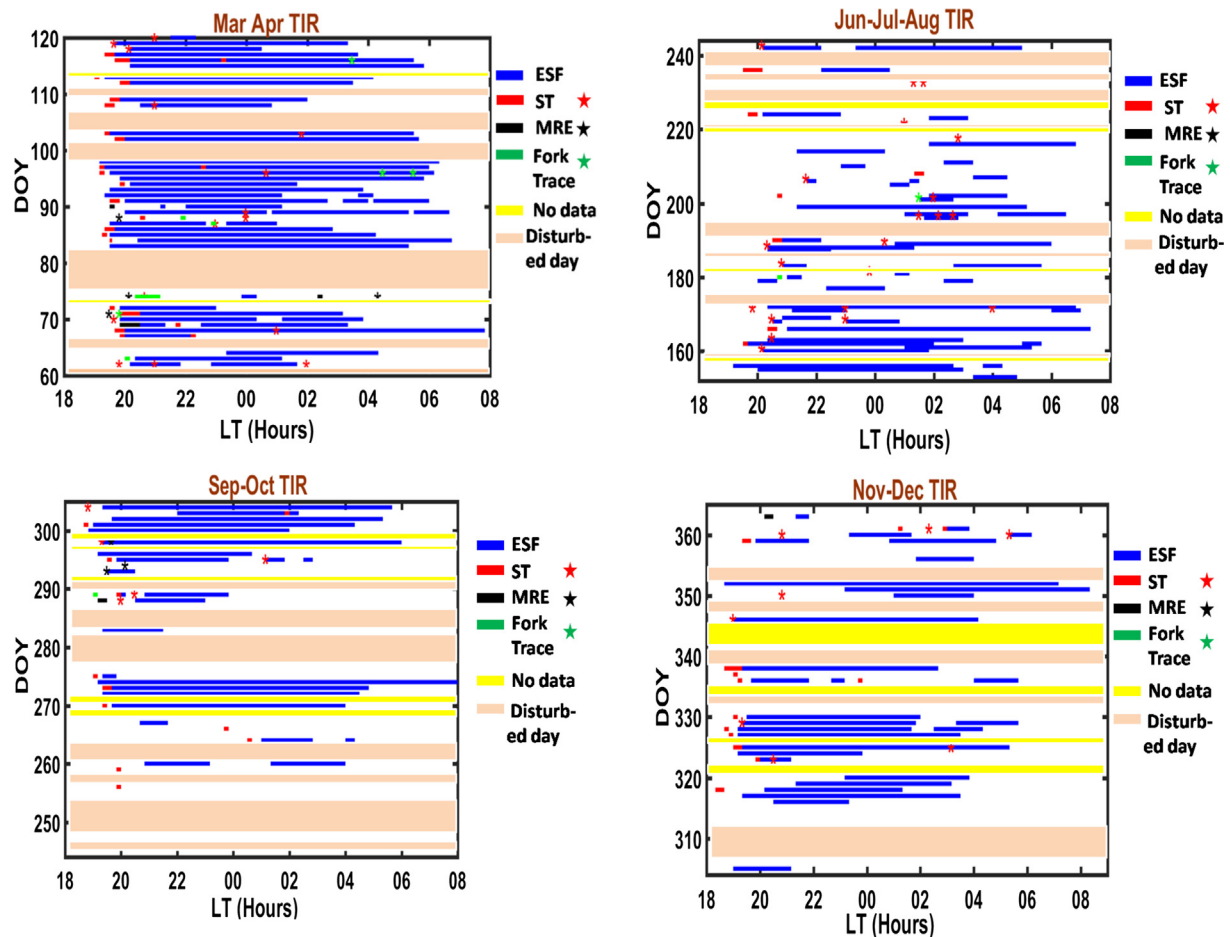
Fig. 4. Ionogram signatures of LSWS at TIR - ST, MRE and Fork traces and occurrence of ESF at TIR (a) during March-April (MA), 2015. (b) Same as (a), but during June-July-August (JJA), 2015. (c) Same as (a), but during September-October (SO), 2015. (d) Same as (a), but during November-December (ND), 2015.

LT = UT+5:30. We focus only on quiet day (Ap < 15) statistics so as to avoid any disturbances interfering the results due to geomagnetic activity. Fig. 4ashows the statistics of ESF as well as ST/MRE/fork traces from TIR during March – April (Vernal) seasons, (4b) June – July – August (Summer) (4c) September – October (Autumn) and (4d) November – December (Winter). From the observations, it can be noted that vernal equinox have majority of days with presence of ESF and most of them are associated with prior appearance of STs. During this season, most of the ESF events initiated in between 19:15 and 20:30 LT. Using the present data, days without ESF are absent during this season. Only a very few number of days show the exception of ESF occurrence without the presence of ST. During summer season, ESF occurred at later hours (around 20:00 LT and later) at TIR. A large variation in the onset time of RSF starting from post-sunset to post-midnight hours during summer months are visible. Here, majority of the ESF events were not preceded by ST during this season. However, Narayanan et al. (2014) reported that the percentage occurrences of ESF following ST was 75% during summer. Li et al. (2011) concluded that although some cases of LSWS/ST that are followed by

spread F occurrence are seen during summer solstice, not all occurrence of spread F at Kwajalein could be associated with LSWS. During Autumn equinox, TIR station has comparatively lesser ESF events than other seasons, especially when compared to vernal (MA) equinox. Here, ESF without ST occurrences were prominent than ESF with ST occurrences. Winter season shows a good number of days preceded by ST, along with a few ESF events with absence of prior STs. Majority of ESF events had onset around 19:00–20:00 LT. When compared to other seasons, vernal (MA) and autumn (SO) equinoxes show a few MRE and fork traces, while other seasons have almost no such cases. A more detailed statistics is presented in the following section.

3.2. Statistical comparison of ESF occurrences and its relation to ST and E_{sb}

Fig. 5a and b gives the statistics of ST (at TIR) on the days of occurrence and non occurrence of ESF at TIR respectively. In Fig. 5a, dark blue shades represent the total no. of ESF days. The corresponding lighter blue shades denote the percentage of days with presence of ST before
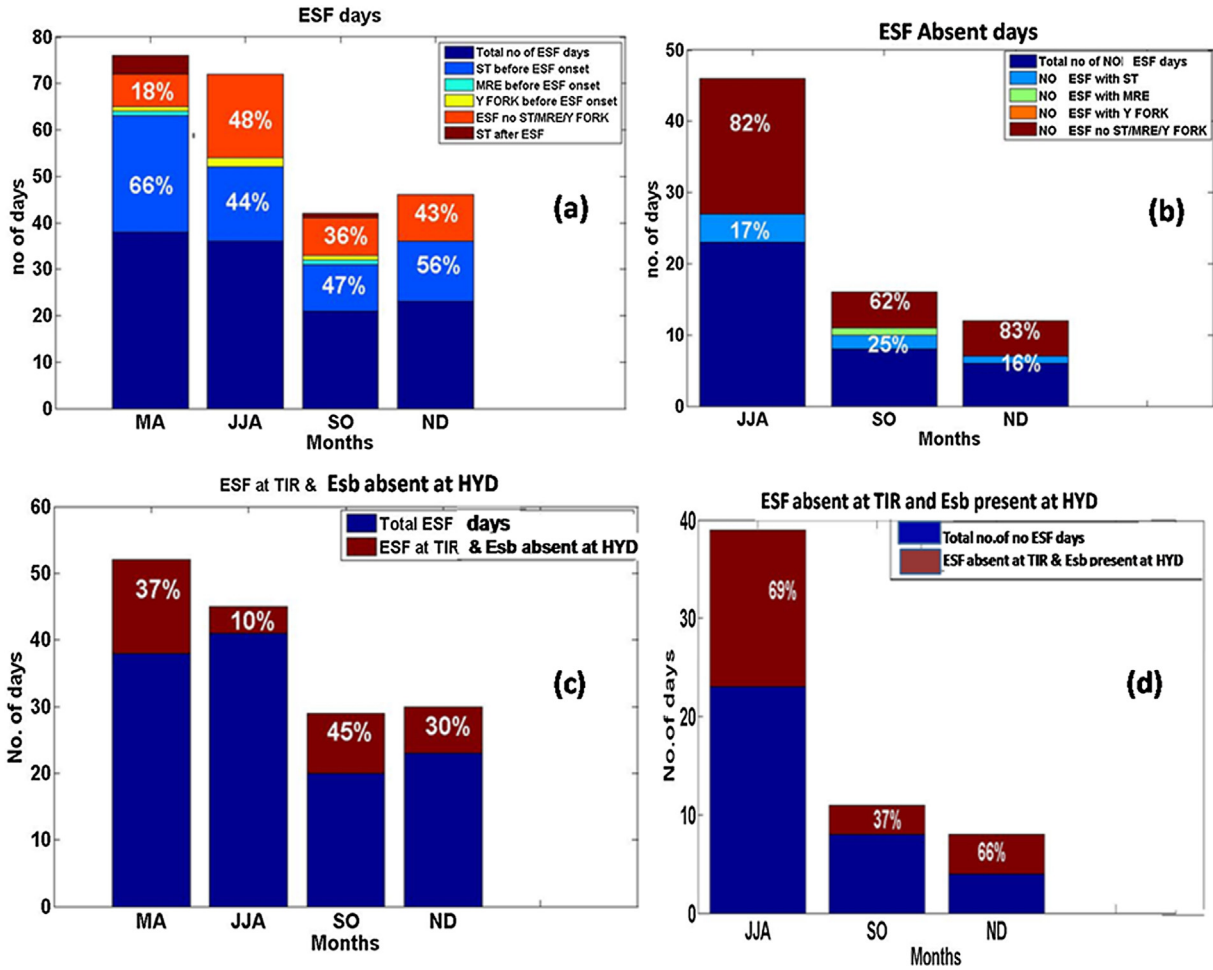
Fig. 5. Statistics of: (a) ESF days at TIR vs ST/MRE/fork traces at TIR during different seasons. (b) Absence of ESF at TIRvs ST/MRE/fork traces at TIR during different seasons. (c) ESF at TIR and E_{sb} absent at HYD during different seasons. (d) ESF absent at TIR and presence of E_{sb} at HYD during different seasons.

ESF onset and those of orange bars denote the percentage of ESF days with absence of prior ST/MRE/Y fork. The results show that the percentage of ESF following ST was highest in March – April (MA) (66%) and least in June – July – August (JJA) (44%). The September – October (SO) season showed nearly same value as JJA. November – December (ND) has 56% ESF days with appearance of ST prior to ESF onset. ESF with absence of prior ST events were least for MA (18%) and highest for JJA (48%). During SO, 36% of ESF events occurred with absence of ST prior to ESF onset, while for ND it was 43%.

It is interesting to note that SO equinox has more number of ESF events with absence of ST before ESF onset than the MA equinox. Based on the statistics of the absence of ESF days during each month (Fig. 5b), JJA and ND months had nearly similar percentages for both cases of absence of ESF days without ST (~82 and 83%) and absence of ESF days with ST (17% and 16%). During MA season, days with absence of ESF was not observed. However, SO season had 62% and 25% of the absence of ESF days without ST and with ST respectively.

Similar statistics is performed in terms of relation of E_{sb} layers in the occurrence/non occurrence of ESF. Two cases were considered such that Fig. 5c and d denotes ESF at TIR/E_{sb} absent over HYD and ESF absent at TIR/E_{sb} present over HYD respectively. It is to be noted that we refer to the ESF at TIR and E_{sb} layers at HYD. It can be seen from Fig. 5c that during ESF days of SO season, about 45% of the ESF events (highest) occurred with the absence of E_{sb} over HYD and the least (10%) was during JJA. MA and ND showed about 37% and 30% of ESF days with E_{sb} absent over HYD. Likewise in Fig. 5d, during the cases of ESF absent days in presence of E_{sb} layers, JJA have majority (69%) of the ESF absent days with E_{sb} present and least (37%) was during SO.

Based on the comparison with MA and SO seasons during the ESF days, it is evident that the percentage of days with presence of ST was higher in MA than SO season. Among the two equinoxes considered in the study, only SO equinox have days with absence of ESF. The percentage of ESF absent days without ST during SO was more (62%) than ESF absent days with E_{sb} present (37%).

3.3. Equinoctial asymmetry in the ESF occurrence - role of STs and E_{sb} layers

In the previous sections, we have dealt with ESF/ absence of ESF cases during all the seasons and the association of ST/E_{sb} in affecting the ESF generation. As seen from the Fig. 5(a–d), a significant equinoctial asymmetry in the ESF occurrence as well as ST occurrence is noted. Hence, further sections are presented such that detailed analysis about the equinoctial asymmetry in the ESF occurrence during the MA (vernal) and SO (autumn) equinoxes are discussed. MA equinox distinctly have majority of ESF events and correspondingly majority of ST occurrences prior to ESF onset than SO equinox. Here, we also study the comparative role of PRE/ST/E_{sb} in a more detailed way which consider day to day cases. Indeed, PRE is an essential factor for ESF. However, it will be interesting to look into various other parameters which can also cause variability of ESF.

Fig. 6a and b shows the temporal variation of virtual height (h'F) at TIR for ESF cases during March-April and September-October months with presence of ST/ MRE/fork traces prior to ESF occurrence. Similarly, Fig. 6c and d refers the same, however with no ionogram signatures of LSWS prior to ESF occurrence. X and Y axis are time and h'F (shown in black colour) at TIR respec-

tively. Dark blue lines denotes ESF duration. Red, green and magenta colours represent the ST, MRE and Fork traces respectively. September-October has nearly equal number of presence and absence of ST cases on these ESF days. However, March – April has majority of ESF days with occurrence of ST prior to ESF onset. It is evident that while there are fewer number of ESF events during March – April with absence of ST before ESF onset, September-October has more number of ESF days with absence of ST before the ESF onset. It is also understood that PRE (h'F max) is higher during March – April than September – October. However, during some days of September-October even with lesser h'F max values presence of ESF is noted.

Fig. 7a and b shows the various parameters considered in the study to understand the asymmetry in the ESF occurrences during March-April and September-October seasons. To begin with, the bottom panel gives the F10.7 solar flux given by 10^{-22} Wm^{-2} Hz^{-1}. The consecutive panels are PRE max (h'F max), number of ionograms STs are observed, presence/absence of E_{sb}, corresponding E_{sb} parameters like ftEs (top frequency) and fbEs (blanketing frequency of E_s layer) respectively. Red and green colour denotes the ESF and post midnight ESF events at TIR respectively. Yellow and black colours represent the disturbed days and data gaps respectively. The average
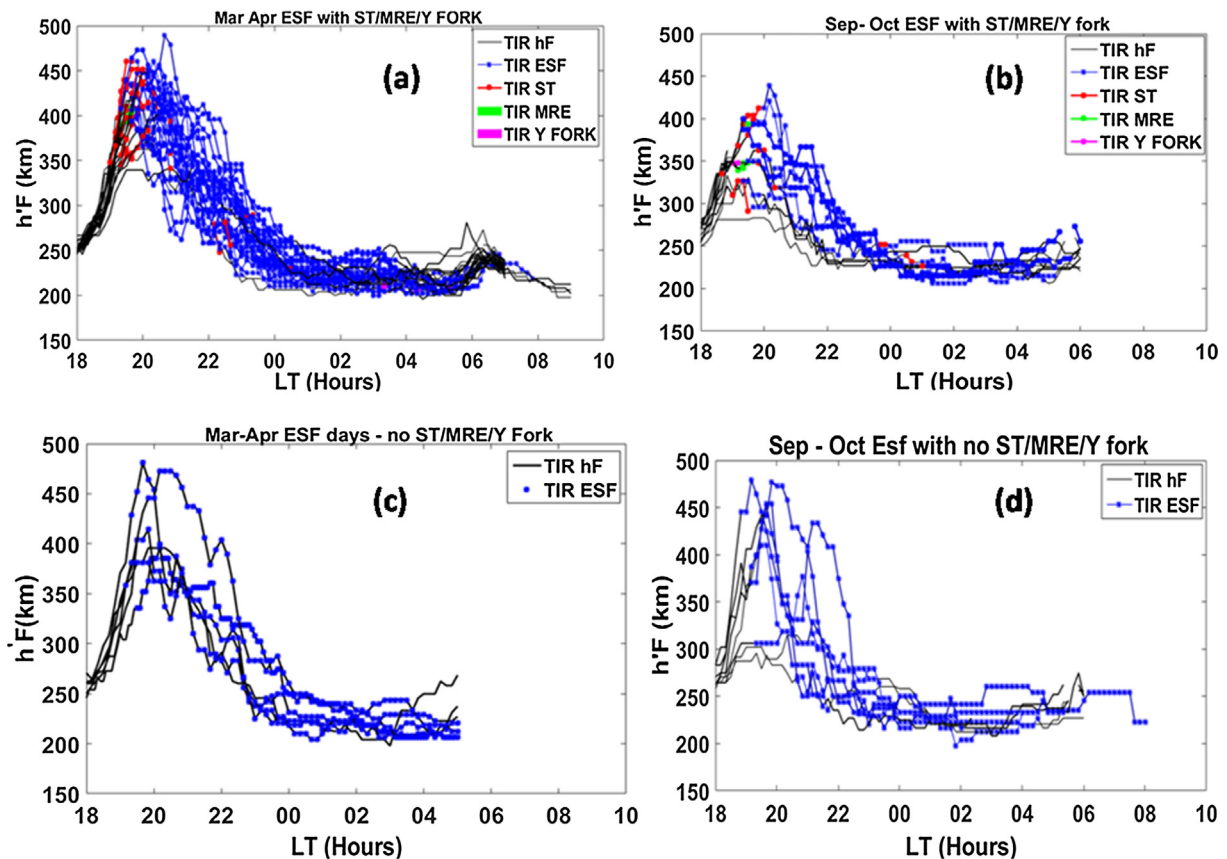

Fig. 6. (a) March-April ESF days with presence of prior ST/MRE/ fork traces. (b) September-October ESF days with presence of prior ST/MRE/ fork traces. (c) March-April ESF days with absence of ST/MRE/ fork traces. (d) September-October ESF days with absence of ST/MRE/ fork traces.
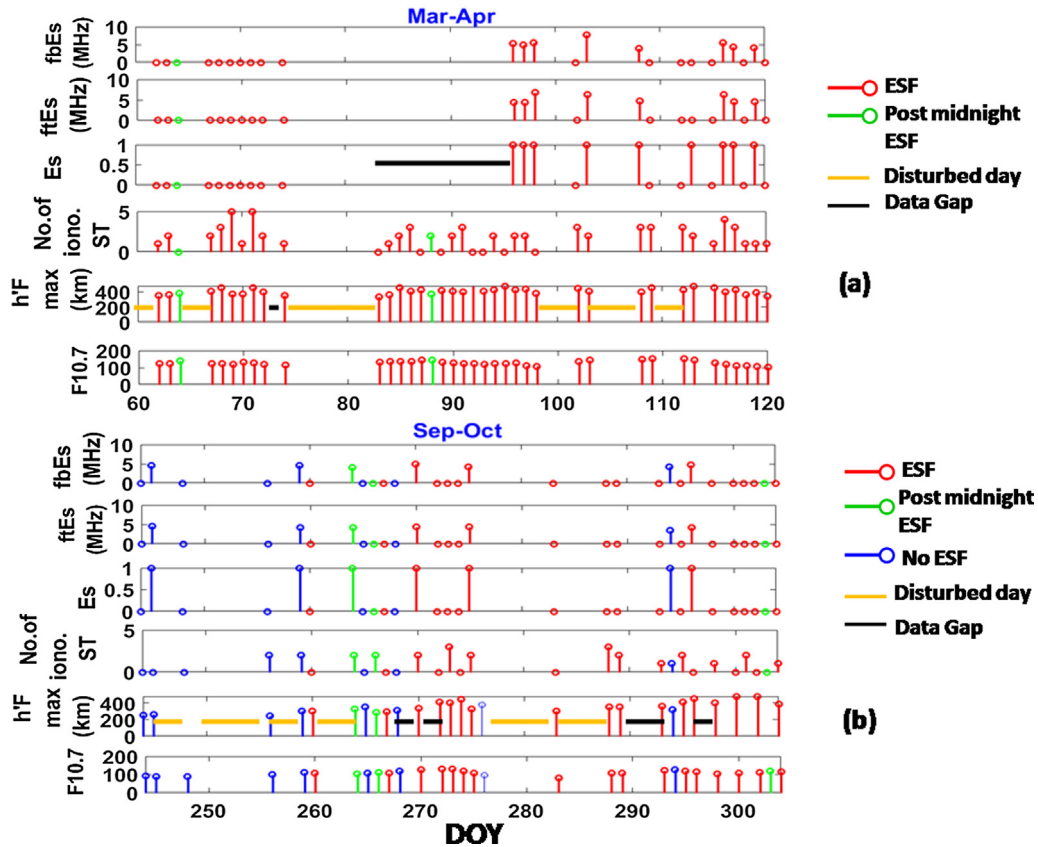
Fig. 7. (a) March-April season: X axis shows day of the year (DOY), Multiple panels on Y axis (from the bottom panel onwards) represent: 1) F 10.7 solar flux (10^{-22} W m^{-2} Hz^{-1}), 2) h'F max (km), 3) number of ionograms in which ST is present, 4) E$_{sb}$ presence/absence, Top frequency of E$_s$ layer (ftE$_s$ (MHz)), 6) Blanketing frequency of E$_{sb}$ layer (fbE$_s$ (MHz)). (b) Same as Fig. (a), but for September-October season.

F10.7 during March – April season is 127 and September-October is 103. From Fig. 7a, it is evident that PRE is high during the March – April, correspondingly h'F max is also high. Apart from this, presence of ST is noted on most of the ESF days. However, absence of ST is seen only for very few days. During early half of the March-April season, presence of ESF is also supported by the absence of E$_{sb}$ at HYD. Although ESF was present in the next few cases, E$_{sb}$ statistics could not be obtained due to the absence of HYD data. The remaining days of the month give mixed response, i.e., ESF days show the presence as well as absence of E$_{sb}$. The non ESF statistics during this season are not studied as all the days were having the presence of ESF.

In Fig. 7b, F10.7 as well as PRE is low during the September-October season and hence h'F max is also low. Although lesser than March – April, during most of the days of the September – October season, ST was present and E$_{sb}$ was absent. Some of the ESF days of September – October are such that PRE is high, however both ST and E$_{sb}$ were absent. During two days in which ESF is seen to be absent, E$_{sb}$ was present with large fbE$_s$ values. It is seen that role of E$_{sb}$ became dominant in those cases where h'F as well as ST are lesser. Another two cases of absence of ESF showed that ST as well as PRE was less with pres-

ence of E$_{sb}$ during a day and absence during another day. E$_{sb}$ was also absent for remaining three non ESF days with higher PRE and absence of ST.

3.4. Characteristics of LSWS during ESF occurrence/non occurrence

While previous sections described the importance of ionogram signatures of LSWS and their statistics in relation to presence/absence of ESF, present section deals with attempts to further confirm the importance of the precursor seed perturbations/LSWS which are believed to be induced by GWs and which can be extracted from the h'F oscillation amplitudes. Virtual height (h'F) values were band-pass filtered to extract their oscillation amplitudes as wave structures within a period band from 1 to 1.5 h. This 1–1.5 h period wave corresponds to ~360 km zonal wavelength of LSWS. The zonal wavelength of these wave structures can be estimated from their period range (which is ~1–1.5 h) and the corresponding phase velocity. As the measurements of phase velocity, V$_p$ are not available, an assumption similar to MacDougall et al. (2011) may be used, i.e., using a phase velocity in the range of 100 m/s, we can obtain a zonal wavelength of ~360 km. The h'F values were obtained at 5, 6 and 7 MHz frequencies.

3.4.1. ESF days

Fig. 8a shows the band-pass filtered h'F values (Dh'F) during March-April at 5, 6 and 7 MHz frequencies from 13:00–20:00 LT (Left panel). The different ESF days used for the study are shown in multiple coloured lines. Vertical drift (dh'F/dt) is calculated for three frequencies separately and the mean of these values for the three frequencies are obtained (shown in right panel as multiple coloured lines for different days). The dashed dark blue curves are the mean of drifts for different days used. The caption of Fig. 8b is same as Fig. 8a, but for ESF days of September-October. Fig. 8a and b present the results of normal ESF days (ESF onset between 19:15 and 20:00 LT) during March-April and September-October respectively. Majority of the events fall in this category. The average ESF onset time for these cases of March – April and September – October is ~19:35 LT and ~19:20 LT respectively. During March-April (Fig. 8a), the average value of peak vertical drift and its time is ~40 m/s and ~19:00 LT respectively.

During September-October (Fig. 8b), the average value of peak vertical drift and its time is ~18: 30 LT and ~30 m/s respectively. During both March-April and September-October ESF days, presence of oscillations of

significant amplitude (Dh'F) in the fixed plasma frequency heights starting from afternoon hours and increasing in amplitude toward sunset is observed. The enhancement being larger for March – April cases as compared to September – October, i.e., the maximum amplitude of oscillations for March – April around post sunset sunset hours is ~12 km and that of September – October is ~6 km. It is hence seen that March-April equinox is having larger wave structure amplitudes and this might suggest the presence of larger amplitude of the seed perturbation which is a key factor in the occurrence of the RT instability.

3.4.2. Early ESF occurrence

Fig. 9a represents the cases of early occurrence of ESF. In this section, we are considering the ESF events which occurred between 18:40 and 19:00 LT. These are some case studies from October month. We did not observe any such cases during March – April and September. The average ESF onset time for the events considered are ~18:45 LT. The description of Fig. 9a remain the same as Fig. 8a and b. During these events, the average value of peak vertical drift and its time is ~18:30 LT and ~45 m/s (right panel). The maximum amplitude of these oscillations
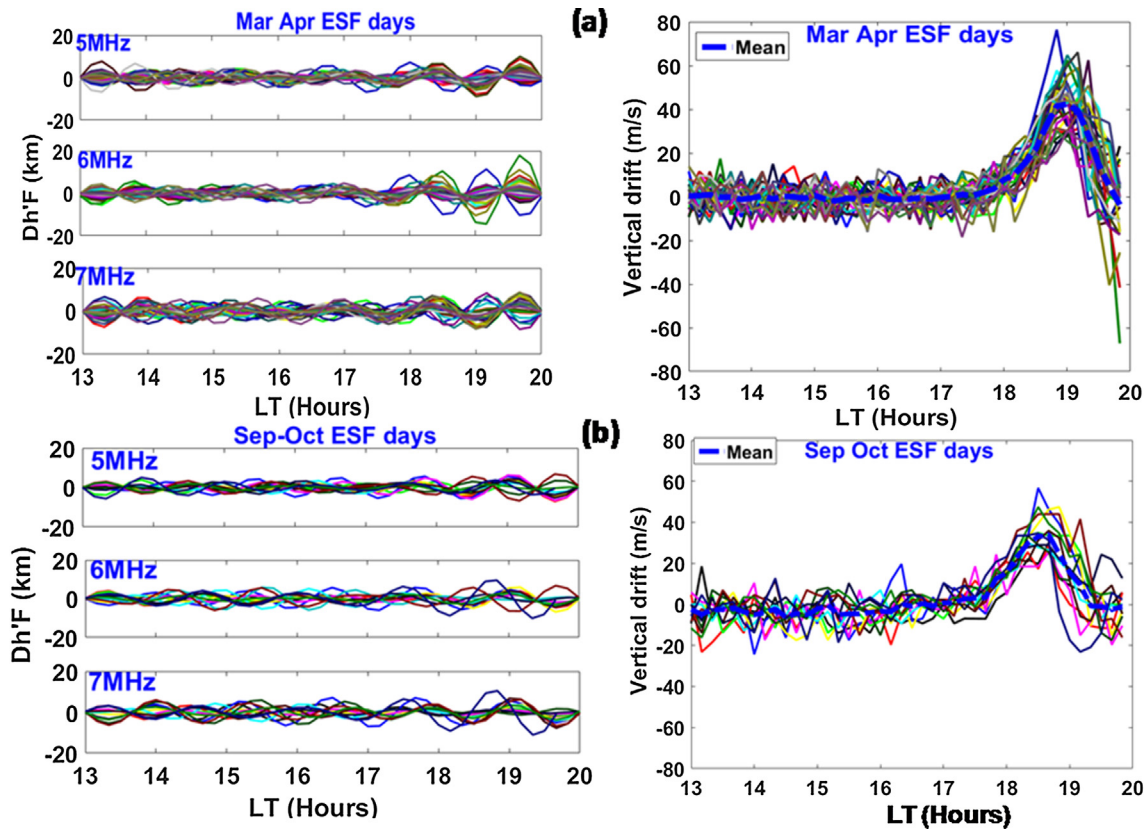

Fig. 8. (a) March-April ESF days: Left panel: Band pass filtered h'F (Dh'F) values for 5, 6 and 7 MHz frequencies. Right panel: Mean of the vertical drifts obtained from 5, 6 and 7 MHz for different ESF days (shown in multiple coloured curves and the mean drift for all the days (dark blue dashed line). The PRE is seen at ~19:00 LT and the average value of peak vertical drift at this time is ~40 m/s. The maximum amplitude of oscillations around post sunset sunset hours is ~12 km. (b) Same as (a), but for September-October ESF days. The average value of peak vertical drift at ~18: 30 LT is ~30 m/s. The maximum amplitude of oscillations around post sunset sunset hours is ~6 km. (For interpretation of the references to colour in this figure legend, the reader is referred to the web version of this article.)
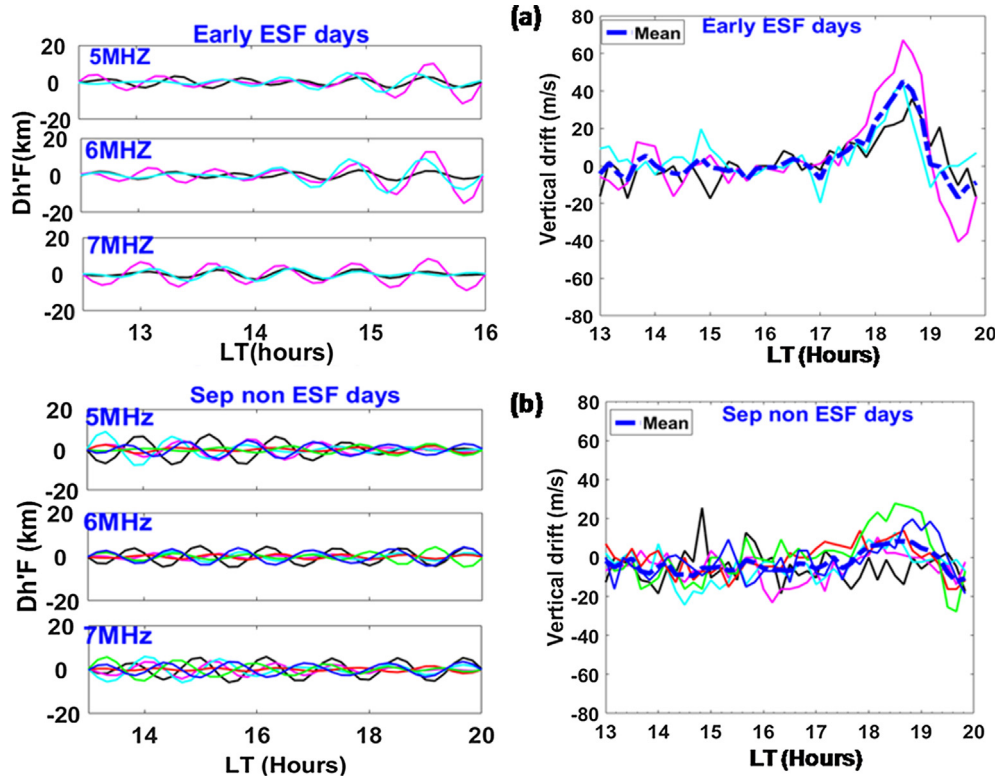
Fig. 9. (a) Same as figure (8), but for Early occurred ESF events. The average value of peak vertical drift and its time is ~18: 30 LT and ~45 m/s. The maximum amplitude of oscillations around post sunset hours is ~12 km. (b) Same as figure (8), but for absence of ESF days during September season. The average value of peak vertical drift and its time is ~18: 40 LT and ~10 m/s. The maximum amplitude of these oscillations around post sunset sunset hours is ~6 km.

around post sunset hours is ~12 km (left panel). Although early ESF and normal ESF days had similar wave structure amplitude, an early occurrence of PRE can be seen during early ESF days.

3.4.3. Absence of ESF

Fig. 9b represent the days from September – October in which ESF did not occur. We did not observe any such cases during March-April. The description of Fig. 9b remain same as Fig. 8a and b. During these events, the average value of peak vertical drift and its time is ~18: 40 LT and ~10 m/s (right panel). The maximum amplitude of these oscillations around post sunset sunset hours is ~6 km (left panel). During the six days of absence of ESF, PRE vertical drifts were significantly smaller than those on the ESF cases. Further, it is seen that absence of ESF cases have generally lower wave structure amplitudes which might suggest that the weak amplitude of the seed perturbation is a key factor in the non occurrence of the RT instability. Hence, it is noticed that both of these pre-cursor conditions (PRE vertical drifts and LSWS (seed)) control the instability growth.

3.4.4. Delayed ESF occurrence

Fig. 10a represents the days in which ESF occurred with a delay during March-April. The events which occurred between 20:00 LT and 21:00 LT are considered in this cat-

egory. Fig. 10b shows the same, but for September-October delayed ESF events. The description of Fig. 10a and b remain same as Fig. 8a and b. From Fig. 10a, the average value of peak vertical drift and its time during March-April is ~19: 00 LT and ~40 m/s (right panel). The average ESF onset time was 20:30 LT. The left panel indicates the maximum enhancement (~6 km) in the oscillation amplitudes around post sunset hours.

Fig. 10b shows the average ESF onset during September-October delayed ESF days as ~20:40 LT, The average vertical drift peak time and value is ~18:40 LT and ~15 m/s. The maximum enhancement in the oscillation amplitudes around post sunset hours as shown in left panel is ~3 km. It is obvious that the oscillation amplitudes are lesser than their corresponding early ESF and normal ESF cases during both equinoxes. Correspondingly, the average drift velocity is also comparatively lesser than previous cases.

Presence of oscillations of significant amplitude (Dh'F) in the fixed plasma frequency heights starting from near noon and increasing in amplitude toward sunset is seen in all the categories discussed above except for the cases in which ESF did not occur.

3.4.5. Signatures of GWs induced LSWS - case studies

Present section discusses the GW propagation characteristics which might give some clues about the
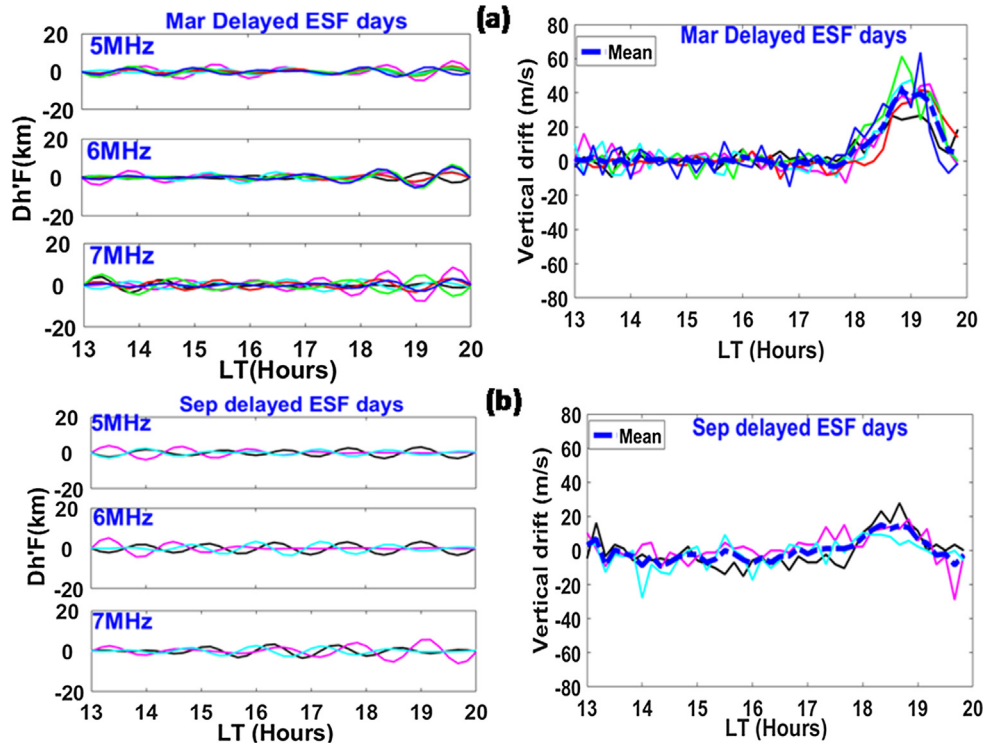
Fig. 10. (a) Same as figure (8), but for delayed occurrence of ESF events during March. The average value of peak vertical drift and its time during March-April is ~19: 00 LT and ~40 m/s. The oscillation amplitude of ~6 km are seen around post sunset hours. (b) Same as figure (8), but for delayed occurrence of ESF events during September. The average vertical drift peak time and value is ~18:40 LT and ~15 m/s. The oscillation amplitudes around post sunset hours is ~3 km.

confirmation of LSWS/ST discussed in previous sections. Fig. 11a represents foF2 values for the fixed heights-250 km, 270 km, 290 km, 310 km, 330 km and 350 km for 3 April 2015 (an ESF day) from 13:00 LT to 19:00 LT. It is seen that the maximum foF2 variations (and hence electron density variations) occur initially at 350 km and later at lower heights, showing a downward phase shift which is characteristic of GW propagation in the ionospheric F region. Slanted black dotted lines indicate the characteristic downward phase propagation. Fig. 11b shows the Fast Fourier Transform (FFT) of the oscillations in the 350 km fixed height value. A time period of 51 min is obtained which is the characteristic of GW propagation.

The vertical phase velocity of the wave, V_z can be calculated from the peak of two consecutive heights (Pezzopane et al., 2011) and V_z is obtained as 23 m/s. The vertical wavelength can be obtained as $\lambda_z = v_z T$. As $T = 51$ min, the vertical wavelength turns out to be, $\lambda_z = 71$ km. The horizontal wavelength (λ_h) can be obtained as:

$$\omega^2 \lambda_h^2 \approx (\omega_g^2 - \omega^2)\lambda_z^2$$

Here, $\omega = 2\Pi/T$ is the wave angular frequency ($T = 51$ min). ω_g, the Brunt –Vaisala frequency is $2\Pi/14$ min^{-1}. From these calculations, the horizontal wavelength, λ_h turns out to ≈ 250 km which is a value consistent with zonal wavelength of LSWS. Similar results may be

obtained for other spread F days as well. Some examples (eg: duing MA equinox) of the presence of ESF, GW and LSWS are shown in the following table.

Date	ESF	Ionogram signature of LSWS
12 March 2015	20:00–02:50	MRE-19:20; ST- 19:50–20:00 Fork trace - 19:40
13 March 2015	19:50–23:00	ST- 19:30–19:50
04 April 2015	20:10–01:40	ST-19:40–20:00
07 April 2015	19:20–05:50	ST-19:10–19:20

The example shown in Fig. 12a and b is on a typical day, 13 September 2015 in which ESF did not occur. Downward phase propagation is not prominent unlike Fig. 11a. A dominant time period is also not observed. This might indicate the absence of GW seed perturbation. Similar results are expected for other cases where spread F did not occur.

4. Discussions

From the observations presented above, it appears that the role of the evening PRE vertical drift is an important factor for the ESF instability growth. However, other factors also contribute to the ESF development such as LSWS as a manifestation of seeding of RT instability, E_{sb} layers
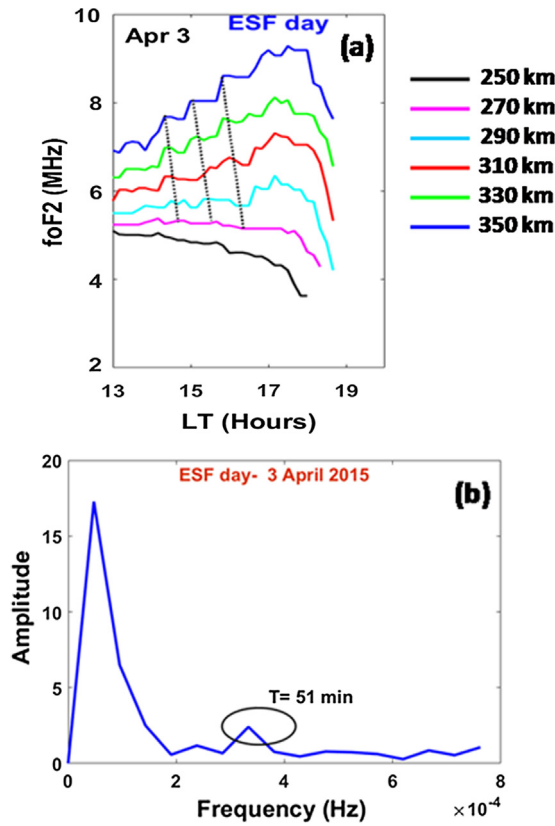
Fig. 11. (a) Frequency variation at fixed heights of 250–350 km on 3 April 2015 (an ESF day) from 13:00 LT to 19:00 LT. Slanted black dotted lines indicate the characteristic downward phase propagation. (b) FFT of the oscillations in the 350 km fixed height value. A time period of 51 min is estimated which is the characteristic of GW propagation.

which can affect the RT instability through its influence in the flux tube integrated conducivities etc. The RT instability growth depend on many factors and hence the study based on only one of the precursors may not give complete information about the ESF variabilities. Hence we attempt to investigate the complementary/competing influence of some of the parameters in influencing ESF development.

One such precursor lies in the large scale wave structures (LSWS) as seen in the bottomside F region. The presence of LSWS has been considered as the earliest manifestation of seed perturbation and their signatures can be seen in ionograms as Satellite Traces (STs), MREs, Fork traces etc (Abdu et al., 1981; Tsunoda, 2008, 2009; Narayanan et al., 2014). Considering the fact that only a fewer number of other two signatures are observed in our study, we carried out this study primarily based on the statistics of STs. It is understood that STs indicate the LSWS in the bottomside electron density distribution. Our investigation of LSWS in terms of STs suggest that while most of the ESF days were preceded by the occurrence of STs during March-April equinox and the least were during June-July-August, most of the ESF absent days were seen to have the absence of STs. Further, it is seen from our observations that though STs and PRE height rise was sufficient
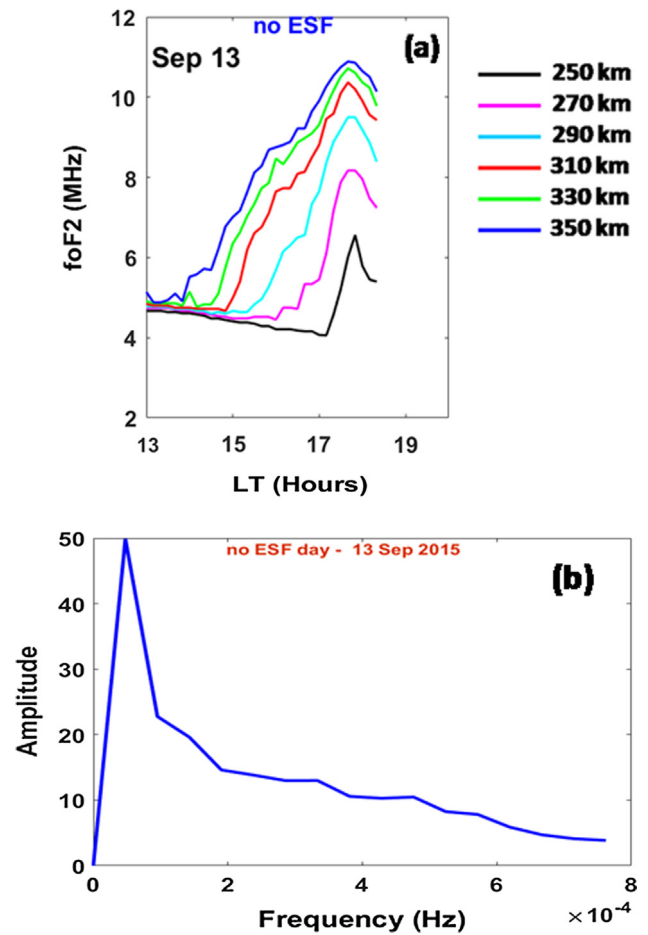

Fig. 12. (a) Frequency variation at fixed heights of 250–350 km on 13 September 2015 (no ESF day) from 13:00 LT to 19:00 LT. Downward phase propagation is not prominent unlike figure (11a). (b) FFT of the oscillations in the 350 km fixed height value. No dominant time period is observed.

near sunset on few days, ESF was not observed. On these days, probably seed amplitude may not be of sufficient strength to initiate the spread F development. Contrary to this, in other cases in which ESF was present, STs were absent in ionograms. The possibility being that the seed amplitude may not be large enough to be detected by ionosonde in the form of 'ST' in ionograms. It should be noted that the presence of ST certainly implies that LSWS signatures are present around sunset. However, the absence of STs on some ESF days may not indicate the absence of LSWS. Such a scenario may possibly happen in those cases also where the resolution of ionosonde is poor. Tsunoda and Ecklund (2007) have investigated the backscatter signal from the bottomside of the F layer using three beam Pohnpei radar and suggested that the LSWS exists during the time of post sunset period. They suggested that since LSWS develops during post sunset through its own eastward polarization electric field, the measured upward drift must be having two components, i.e., one associated with PRE, and the other associated with LSWS. Based on this finding, they indicated that the distinction of two components of vertical drifts in terms of LSWS and PRE

on a day-to-day basis may be the key to understand day-to-day variability in ESF irregularities. Contrary to the one to one correspondence of LSWS and ESF reported by earlier workers, more recently it has been shown that in some cases, LSWS appeared but without any subsequent ESF development (Li et al., 2012; Narayanan et al., 2012). A few individual events in the present work is in agreement with their study. Thampi et al. (2009) reported that the presence of LSWS is a important pre-requisite for the subsequent development of ESF.

Apart from the aforementioned influence of STs, E_{sb} layers can also be a contributor to the variability in ESF occurrence. The influence of the low latitude E region conductivity around sunset in causing the day-to-day variability of the ESF irregularities through changes in flux tube–integrated conductivity are investigated widely (Bhattacharyya, 2004). It is believed that electron density convergence/divergence leading to the E_s layer formation/disruption could be driven by a vertical Hall electric field, induced by the primary zonal electric field in the presence of enhanced ratio of field line integrated Hall to Pedersen conductivity $(\Sigma H)/(\Sigma P)$ (Abdu et al., 2003). Stephan et al. (2002) have examined the role of sporadic E layers at low-latitude on the development of ESF through the changes in the flux tube–integrated conductivity. They found that the growth rate of RT instability to be lowered by an order of magnitude when sporadic E layer density is of the order 1×10^6 cm^3. Hence, small increase in the post sunset E region electron density could lead to a significant suppression of ESF through reduction in the upward plasma drift.

The statistics obtained by comparing both the factors, ST and E_{sb} during the four seasons reveal interesting results. Based on these findings, it is evident that during ESF days in all the seasons, percentage of presence of ST over TIR is dominating when compared to the percentage of absence of E_{sb} over HYD. Further, during the absence of ESF events, the percentage of absence of ST is higher than the percentage of presence of E_{sb} during the seasons studied for the year. This probably indicate that the presence/absence of ST in providing seed perturbation might have more significance than absence/presence of E_{sb} resulting in generation/suppression of ESF irregularities. Additionally, the results of non-correlation of low latitude E_{sb} layers with ESF possibly may indicate its coupling to higher apex altitudes over the equator than needed. This might be due to the fact that Es layers at HYD and its connection to base of F layer might also have solar flux influence. Depending upon the height of the base of F layer in the evening hours, Es layers at HYD may influence. If solar flux is very strong, i.e., high solar activity period, then F layer base may connect to Es layers at higher latitudes. But under low solar activity period, as base height of the F layer is very low, then HYD Es layers may not connect to base of the F layer.

Another interesting feature presented in our study is the equinoctial asymmetry in the occurrence of ESF irregularities observed during the year 2015, i.e., vernal equinox

seems to have more number of occurrences of ST and ESF than autumn equinox. Hence, one of the important highlights of the study is to understand this asymmetry in terms of ST occurrences (as a proxy for LSWS) and low latitude E_{sb} layers. Based on the examination of solar flux differences between vernal (127) and autumn equinox (103), we see small differences in their values with vernal equinox being higher in value than autumn equinox. Correspondingly, PRE values also reveal such a similar enhancement. In the recent past, based on VHF/GPS TEC and scintillations from Indian sector, Sripathi et al. (2011) reported the equinoctial asymmetry in the occurrence of scintillation and ROTI (ROTI (Rate of TEC index) is a widely used index with the ionospheric irregularities level is measured and it is defined as the standard deviation of the ROT (Rate Of TEC) over some time interval). They attributed that the height of F layer is higher during vernal equinox as compared to autumn equinoxes. In general, it can be understood that the differences in the solar flux dependence of vertical drift during MA and SO equinoxes might be associated with the differences in neutral wind, background ionospheric conductivities and conductivity gradient near sunset terminator during these two equinoxes. However along with that, the seeding as well as the presence/absence of E_{sb} also might have had a contribution to the differences in ESF over the two equinoxes. Our observations suggested that percentage of ST prior to occurrence of ESF cases is more than half in overall cases during MA equinox. Narayanan et al. (2014) reported that the percentage of ST prior to ESF cases was higher in summer solstice and during later hours of night. The differences in the amplitude of seed perturbation during seasons of different years might be responsible for this particular difference in observation. It is also seen that more than the presence/absence of E_{sb}, weak/insufficient as well as no ST/no LSWS scenario may result in suppression of ESF on some days.

More precisely, day to day case studies during MA and SO reveal evidences for the competing/complementary influence of PRE, ST and E_{sb} layers. The primary factor, PRE shows significance during MA than SO and hence h'F max values are also correspondingly higher. While most of the days during MA were associated with presence of STs, only a few days were observed with the absence of STs. However, E_{sb} gives more or less a mixed response. This suggests that PRE along with sufficiently higher percentage of presence of STs might be associated with the ESF generation on most of the days. During SO, out of the 8 non ESF days, 3 days showed the presence of strong E_{sb} layers in the presence of high PRE and presence of ST. However, 5 of the remaining days revealed the absence of ST. Joshi et al. (2013) suggested that ESF occurred (did not occur) irrespective of E_s type if the virtual height of the F layer base (h'F) was greater than $\sim$360 km (less than $\sim$290 km) and ESF occurrence depended strongly on the type of E_s if 290 km < h'F < 360 km. Hence, E_s could play important role in the cases when F layer height is not very high. It can be further explained that if the height of F layer

is beyond a certain threshold, then correspondingly ion neutral collision (ν_{in}) frequency will be low enough (thereby greater reduction in the conductivity ratio) such that RT instability will be higher. As a result, these processes can hence cancel the effect produced by low latitude E_s layers. Joshi et al. (2013) have considered another low latitude station, SHAR (13.74°N, 80.20°E, geomag: 6.7° N) for their study which is closer to equator than HYD, while present study carries out the E_{sb} observations from HYD. Hence the latitudinal differences might have also played role in the differences in E_{sb} observations. However, Batista et al. (2008) reported that the presence of E_s at the conjugate sites is neither a necessary nor a sufficient condition for the inhibition of ESF at the magnetic equator. However, present analysis suggests that during this period of study, it seems the dominance of ST/LSWS over E_{sb} is contributing for ESF variabilities. Since SHAR is very close to equator than HYD, the E_s layers at SHAR may be well connected to the base of F region. Contrary to this, HYD is located slightly far away from the equator that possibly connect to higher altitudes than base of F region. Accordingly, the absence of good correlation in our results may be justified.

Till now, the role of STs in the variability of ESF occurrence are discussed. While STs are signatures of LSWS arising from visual inspection of ionograms during post sunset hours, the presence of LSWS can be seen as GW induced wave structures manifesting itself as the height oscillations of the bottomside F layer during daytime. Hence, further investigations are carried out so as to confirm the role of STs/LSWS in causing the equinoctial asymmetry of ESF which reveal interesting results. However, our study not only rely on visually observed STs, but as a confirmation to those STs, we analyzed the h'F values scaled for different frequencies. The band pass filtered h'F values obtained for three fixed frequencies showed the presence of oscillations/wave like structures (period of 1–1.5 h) which initiates well before sunset. Our observation suggests that although the oscillation amplitude is less during afternoon hours, enhancement occurs at a later stage during the post sunset hours of ESF days.

Based on diagnostics by a digisonde and a VHF radar, Abdu et al. (2009) showed that the amplitude of the GW-induced wavelike structures in the F layer heights during presunset hours that continued their development into postsunset ESF growth was dependent on the amplitude of the PRE vertical drift. Such precursor wave structures are identifiable as LSWS. Earlier investigators also reported that the large-scale modulation is partially due to spatially resonant atmospheric GWs and the amplification of seed perturbation is by the Rayleigh-Taylor instability (Kelley et al., 1981). Later, based on an observational study from Brazilian equatorial sector, Abdu et al. (2015) presented the GW-induced wave structures in polarization electric field seen in the form of F layer height oscillations produced by the vertical or zonal perturbation winds. It is believed that atmospheric GWs

can cause neutral wind perturbations in the F region which can result in the generation of spatially varying dynamo current and they can be regarded as the cause of generation of LSWS (Tsunoda et al., 2011). Recently, Li et al. (2017) studied the presence of F region bottom-type irregularity layer well before sunset in southeast Asia. They reported that similar oscillations were found in the Doppler velocities of the pre-sunset bottom-type irregularity echoes (measured by radar) and the F layer heights (obtained from digisonde) providing further evidence on the pre-sunset polarization electric field.

Moreover, it is well known that during post sunset hours, E region recombination happens and as a result sharp decrease in E region conductivity occurs, which further increases the ratio of F to E region conductivity. PRE, which is the result of F region dynamo existing at post sunset hours further causes the uplift of the F layer. This thereby enhances the growth of oscillations through RT instability process. As understood from our results, a clear correlation between temporal oscillations of height and PRE vertical drift is noticed, i.e., larger filtered h'F oscillation amplitudes are seen in conjunction with a larger evening vertical drift (PRE) as well as smaller oscillation amplitudes are seen in conjunction with a smaller evening vertical drift (PRE). This observation is consistent in all the cases of ESF as well as ESF absent cases discussed in the study. Particularly, the enhancement of oscillation amplitude in conjunction with enhancement in the PRE drift during MA ESF days when compared to SO cases strengthens the point of statistical observation of more number of STs prior to ESF during MA season as compared to SO. Additionally, the smaller oscillation amplitudes along with smaller vertical drift on ESF absent days as compared to ESF days during SO might suggests the significance of LSWS in addition to PRE in influencing the ESF variabilities. More interestingly, such enhanced amplitudes were also observed for early ESF events when compared to delayed ESF occurrences.

However, it may be mentioned that the significant amplification of LSWS may not be solely attributed to the PRE electric fields. Abdu et al. (2015) suggested that the spatial resonance mechanism is also considered as responsible for the enhancement in oscillation amplitude. Under this condition, density or polarization electric field perturbation amplitudes can be enhanced. This can affect the growth of seed which can result in RT instability growth during post sunset hours under favourable background conditions. Hence, our results suggest that height increase of F layer due to PRE, along with the presence of LSWS might have provided suitable conditions for ESF development. They also reported an investigation of these precursor wave structures for ESF and non ESF events during Autumn equinox. Their study was carried out for Brazilian equatorial stations. However to the best of our knowledge, this kind of classification study of filtered h'F oscillations so as to investigate the importance of LSWS in equinoctial asymmetry in ST occurrence and

also in early and delayed ESF events are not much reported previously. Moreover, Abdu et al. (2015) concluded that this kind of precursor wave characteristics study can be extended to other longitude sectors as well. Hence, we believe that our study from the Indian sector turns out to be a further verification of this fact.

The analysis of foF2 values for fixed height ranges of 250–350 km verifies the presence of GWs as a source for these wave structures. An evident downward phase propagation (Alfonsi et al. (2013)) (characteristic of GWs) was observed on the ESF day with a time period of 51 min and horizontal wavelength of ∼250 km is calculated. These values are nearly consistent with the wave structures obtained as oscillations in the filtered h'F values. However, such a downward phase propagation characteristic and time period was absent on the day in which ESF was absent. From ALTAIR incoherent scatter radar observations, Tsunoda and White (1981) have shown that the zonal wavelengths of LSWS vary around 300–600 km. The zonal scale size of the wave structures ranging from 400 to 1200 km is also reported also by (Thampi et al., 2009; Abdu et al., 2009). Later on, using differential phase technique to derive the zonal LSWS from the CERTO beacon transmissions of C/NOFS, Tulasi Ram et al. (2012) reported various characteristics of LSWS. They found that zonal wavelengths of wavelike structures are found to vary in the range 250–615 km and these zonal wave structures are LSWS in the bottom side F region.

Although we presented some evidences for the role of STs/LSWS and E_{sb} layers in affecting variability of ESF irregularities, due to the lack of simultaneous observations of these wave structures longitudinally, we are not able to explain some of the observations which can be investigated by using the latitudinal and longitudinal chain of ionosondes to detect STs and E_{sb} layers. Once we have such network in place, we shall be able to bring more advancements in the study of significance of LSWS and E_{sb} layers in causing the day-to-day variability of ESF irregularities.

5. Conclusions

In this work, we studied the statistics of equatorial STs (an ionogram signature of LSWS) and E_{sb} layers over low latitude in addition to PRE as factors so as to understand their role in affecting the variabilites in ESF generation.

The main points of the study are summarized as follows:

(1) The statistics of ST and E_{sb} estimated during different seasons of 2015 suggest that STs preceding the ESF was highest (66%) during vernal equinox (March-April) season and least (44%) during summer (June-July-August) season, which is found to be in contrast with previous studies.

(2) Significant equinoctial asymmetries in the ESF occurrences as well as ST/LSWS occurrences were seen during the year, i.e., while vernal equinox have more number of ESF cases preceded by ST, autumn equinox shows comparatively lesser number of such cases.

(3) During all the seasons, it is seen that percentage of ST prior to ESF occurrence is higher than the corresponding percentage of absence of E_{sb} during the same season. Similarly, the percentage of absence of ST during the post sunset hours on ESF absent days are higher than the percentage of presence of E_{sb} around the sunset hours. This might imply the importance of ST/LSWS in influencing the ESF generation rather than low latitude E_{sb} layers.

(4) Oscillation amplitudes obtained from band pass filtered h'F values using fixed frequencies suggest that although the oscillation amplitudes are present even in the late afternoon hours, their enhancement occurred only during post sunset hours. This enhancement near the post sunset hours, in conjunction with enhancement in the PRE drift during ESF days of MA when compared to that of SO cases strengthens and validates the point of large number of STs observed prior to ESF during MA season as compared to SO.

(5) Additionally during the post sunset hours, the smaller oscillation amplitudes along with smaller vertical drift values during the days of absence of ESF as compared to ESF days of SO and enhanced amplitudes for early ESF events when compared to delayed ESF occurrences are seen. This might suggests that F layer height rise (induced by the PRE), together with the presence of LSWS provide suitable conditions for the ESF development.

(6) The presence of downward phase propagation as well as a time period of 51 min seen on ESF days when compared to the days of absence of ESF clearly marks the role of upward propagating GWs in the initiation of these wave structures.

References

Abdu, M.A., Batista, I.S., Bittencourt, J.A., 1981. Some characteristics of spread F at the magnetic equatorial station Fortaleza. J. Geophys. Res. 86, 6836–6842.

Abdu, M.A., Medeiros, R.T., Sobral, J.H.A., Bittencourt, J.A., 1983. Spread F plasma vertical rise velocities determined from spaced ionosonde observations. J. Geophys. Res. 88 (9197–9204), 1983.

Abdu, M.A., MacDougall, J.W., Batista, I.S., Sobral, J.H.A., Jayachandran, P.T., 2003. Equatorial evening prereversal electric field enhancement and sporadic E layer disruption: A manifestation of E and F region coupling. J. Geophys. Res. 108 (A6), 1254. https://doi.org/10.1029/2002JA009285, 2003.

Abdu, M.A., Alam Kherani, E., Batista, I.S., de Paula, E.R., Fritts, D.C., Sobral, J.H.A., 2009. Gravity wave initiation of equatorial spread F/plasma bubble irregularities based on observational data from the SpreadFEx campaign. Ann. Geophys. 27, 2607–2622. https://doi.org/10.5194/angeo-27-2607-2009.

Abdu, M.A., de Souza, J.R., Kherani, E.A., Batista, I.S., MacDougall, J.W., Sobral, J.H.A., 2015. Wave structure and polarization electric field development in the bottomside F layer leading to postsunset equatorial spread F. J. Geophys. Res. Space Phys. 120, 6930–6940. https://doi.org/10.1002/2015JA021235.

Alfonsi, L., Spogli, L., Pezzopane, M., Romano, V., Zuccheretti, E., De Franceschi, G., Cabrera, M.A., Ezquer, R.G., 2013. Comparative analysis of spread-F signature and GPS scintillation occurrences at Tucuma'n, Argentina. J. Geophys. Res. Space Phys. 118, 4483–4502. https://doi.org/10.1002/jgra.50378.

Batista, I.S., Abdu, M.A., Carrasco, A.J., Reinisch, B.W., de Paula, E.R., Schuch, N.J., Bertoni, F., 2008. Equatorial spread F and sporadic E-layer connections during the Brazilian Conjugate Point Equatorial Experiment –COPEX. J. Atmos. Sol. Terr. Phys. 70, 1133–1143. https://doi.org/10.1016/j.jastp.2008.01.007.

Bhattacharyya, A., 2004. Role of E region conductivity in the development of equatorial ionospheric plasma bubbles. Geophys. Res. Lett. 31, L06806. https://doi.org/10.1029/2003GL018960.

Fejer, B.G., Scherliess, L., de Paula, E.R., 1999. Effects of the vertical plasma drift velocity on the generation and evolution of equatorial spread F. J. Geophys. Res. 104, pp. 19,854–19,869.

Joshi, L.M., Patra, A.K., Rao, S.V.B., 2013. Low-latitude E_s capable of controlling the onset of equatorial spread F. J. Geophys. Res. Space Phys. 118, 1170–1179. https://doi.org/10.1002/jgra.50189.

Kelley, M.C., Makela, J.J., de La Beaujardière, O., Retterer, J., 2011. Convective ionospheric storms: A review. Rev. Geophys. 49, RG2003, doi:10.1029/2010RG000340

Kelley, M.C., Larsen, M.F., LaHoz, C.A., McClure, J.P., 1981. Gravity wave initiation of equatorial spread F: A case study. J. Geophys. Res. 86, 9087–9100. https://doi.org/10.1029/JA086iA11p09087.

Kherani, E.A., Abdu, M.A., de Paula, E.R., Fritts, D.C., Sobral, J.H.A., de Meness, Jr.F.C., 2009. The impact of gravity waves rising from convection in the lower atmosphere on the generation and nonlinear evolution of equatorial bubble. Ann. Geophys. 27, 1657–1668. https://doi.org/10.5194/angeo-27-1657-2009.

Li, G., Ning, B., Abdu, M.A., Yue, X., Liu, L., Wan, W., Hu, L., 2011. On the occurrence of postmidnight equatorial F region irregularities during the June solstice. J. Geophys. Res. 116, A04318. https://doi.org/10.1029/2010JA016056.

Li, G., Ning, B., Abdu, M.A., Wan, W., Hu, L., 2012. Precursor signatures and evolution of post-sunset equatorial spread-F observed over Sanya. J. Geophys. Res. 117, A08321. https://doi.org/10.1029/2012JA017820.

Li, G., Otsuka, Y., Ning, B., Abdu, M.A., Yamamoto, M., Wan, W., Liu, L., Abadi, P., 2016. Enhanced ionospheric plasma bubble generation in more active ITCZ. Geophys. Res. Lett. 43, 2389–2395. https://doi.org/10.1002/2016GL068145.

Li, G., Ning, B., Abdu, M.A., Wan, W., Wang, C., Yang, G., Liu, K., Liu, L., Yan, C., 2017. First observation of presunset ionospheric F region

bottomtype scattering layer. J. Geophys. Res. Space Phys. 122, 3788–3797. https://doi.org/10.1002/2016JA02364.

Lyon, A.J., Skinner, N.J., Wright, R.W., 1961. Equatorial spread-F at Ibadan, Nigeria. J. Atmos. Terr. Phys. 21, 100–119.

Maruyama, T., 1988. A diagnostic model for equatorial spread F, 1. Model description and application to electric field and neutral wind effects. J. Geophys., Res., 93(A12), pp. 14611–14622.

Narayanan, V.L., Taori, A., Patra, A.K., Emperumal, K., Gurubaran, S., 2012. On the importance of wave-like structures in the occurrence of equatorial plasma bubbles: A case study. J. Geophys. Res. 117, A01306. https://doi.org/10.1029/2011JA017054.

Narayanan, V.L., Sau, S., Gurubaran, S., Shiokawa, K., Balan, N., Emperumal, K., 2014. A statistical study of satellite traces and subsequent evolution of equatorial spread F based on ionosonde observations over dip equatorial site Tirunelveli, India. Earth Planets Space 66, 160.

Manju, G., Madhav Haridas, M.K., Aswathy, R.P., 2016. Role of gravity wave seed perturbations on ESF day-to-day variability: A quantitative approach. Adv. Space Res. 57, 1021–1028.

MacDougall, J., Abdu, M.A., Batista, I., Buriti, R., Medeiros, A.F., Jayachandran, P.T., Borba, G., 2011. Spaced transmitter measurements of medium scale traveling ionospheric disturbances near the equator. Geophys. Res. Lett. 38, L16806. https://doi.org/10.1029/2011GL048598.

Patra, A.K., Taori, A., Chaitanya, P.P., Sripathi, S., 2013. Direct detection of wavelike spatial structure at the bottom of the F region and its role on the formation of equatorial plasma bubble. J. Geophys. Res. Space Phys. 118, pp. 1196–1202, doi:10.1002/jgra.50148.

Pezzopane, M., Fagundes, P.R., Ciraolo, L., Correia, E., Cabrera, M.A., Ezquer, R.G., 2011. Unusual nighttime impulsive foF2 enhancement below the southern anomaly crest under geomagnetically quiet conditions. J. Geophys. Res. 116, A12314. https://doi.org/10.1029/2011JA016593.

Saito, S., Maruyama, T., 2007. Large-scale longitudinal variation in ionospheric height and equatorial spread F occurrences observed by ionosondes. Geophys. Res. Lett. 34, L16109. https://doi.org/10.1029/2007GL030618.

Sreeja, V., Vineeth, C., Pant, T.K., Ravindran, S., Sridharan, R., 2009. Role of gravity wavelike seed perturbations on the triggering of ESF—First results from unique day glow observations. Ann. Geophys. 27, pp. 313–318.

Sripathi, S., Kakad, B., Bhattacharyya, A., 2011. Study of equinoctial asymmetry in the Equatorial Spread F (ESF) irregularities over Indian region using multi-instrument observations in the descending phase of solar cycle 23. J. Geophys. Res. 116, A11302. https://doi.org/10.1029/2011JA016625.

Stephan, A.W., Colerico, M., Mendillo, M., Reinisch, B.W., Anderson, D., 2002. Suppression of equatorial spread F by sporadic E. J. Geophys. Res. 107, 1021. https://doi.org/10.1029/2001JA000162.

Takahashi, H., Taylor, M.J., Pautet, P.-D., Medeiros, A.F., Gobbi, D., Wrasse, C.M., Fechine, J., Abdu, M.A., Batista, I.S., Paula, E., Sobral, J.H.A., Arruda, D., Vadas, S.L., Sabbas, F.S., Fritts, D.C., 2009. Simultaneous observation of ionospheric plasma bubbles and mesospheric gravity waves during the SpreadFEx campaign. Ann. Geophys. 27, pp. 1477–1487, doi:10.5194/angeo-27-1477-2009.

Taori, A., Makela, J.J., Taylor, M., 2010. Mesospheric wave signatures and equatorial plasma bubbles: A case study. J. Geophys. Res. 115, A06302, doi:10.1029/2009JA015088.

Thampi, S.V., Yamamoto, M., Tsunoda, R.T., Otsuka, Y., Tsugawa, T., Uemoto, J., Ishii, M., 2009. First observations of large-scale wave structure and equatorial spread F using CERTO radio beacon on the C/NOFS satellite. Geophys. Res. Lett. 36, L18111. https://doi.org/10.1029/2009GL039887.

Thampi, S.V., Tsunoda, R.T., Jose, L., Pant, T.K., 2012. Ionogram signatures of large-scale wave structure and their relation to equatorial spread F. J. Geophys. Res. 117, A08314. https://doi.org/10.1029/2012JA017592.

Tsunoda, R.T., White, B.R., 1981. On the generation and growth of equatorial backscatter plumes: 1. Wave structure in the bottomside F layer. J. Geophys. Res. 86, 3610–3616. https://doi.org/10.1029/JA086iA05p03610.

Tsunoda, R.T., 2005. On the enigma of day-to-day variability in equatorial spread F. Geophys. Res. Lett. 32, L08103. https://doi.org/10.1029/2005GL022512.

Tsunoda, R.T., Ecklund, W.L., 2007. On the post-sunset rise of the equatorial F layer and superposed upwellings and bubbles. Geophys. Res. Lett. 34, L04101. https://doi.org/10.1029/2006GL028832.

Tsunoda, R.T., 2008. Satellite traces: An ionogram signature for large-scale wave structure and a precursor for equatorial spread F. Geophys. Res. Lett. 35, L20110. https://doi.org/10.1029/2008GL035706.

Tsunoda, R.T., 2009. Multi-reflected echoes: Another ionogram signature of large-scale wave structure. Geophys. Res. Lett. 36, L01102. https://doi.org/10.1029/2008GL036221.

Tsunoda, R.T., Yamamoto, M., Tsugawa, T., Hoang, T.L., Tulasi Ram, S., Thampi, S.V., Chau, H.D., Nagatsuma, T., 2011. On seeding large-scale wave structure, equatorial spread F, and scintillations over Vietnam. Geophys. Res. Lett. 38, L20102. https://doi.org/10.1029/2011GL049173.

Tsunoda, R.T., 2012. A simple model to relate ionogram signatures to large-scale wave structure. Geophys. Res. Lett. 39. https://doi.org/10.1029/2012GL053179.

Tulasi Ram, S., Yamamoto, M., Tsunoda, R.T., Thampi, S.V., Gurubaran, S., 2012. On the application of differential phase measurements to study the zonal large scale wave structure (LSWS) in the ionospheric electron content. Radio Sci. 47, RS2001, doi:10.1029/2011RS004870.